Floating, Highly Efficient, and Scalable Graphene Membranes for Seawater Desalination using Solar Energy

Guijun Li, Wing Cheung Law and Kang Cheung Chan*

Advanced Manufacturing Technology Research Centre

Department of Industrial and Systems Engineering

Hong Kong Polytechnic University, Hong Kong

*E-mail: kc.chan@polyu.edu.hk

Abstract

Seawater dehydrates humans when it is drunk untreated, due to its high concentrations of salts. Currently, it can only be purified into large amounts of freshwater using reverse osmosis, with large electricity consumption, carbon emissions and environmental damage. Although seawater directly evaporates under natural sunlight, the efficiencies and scales are too small for practical collection. Herein, we report a floating graphene membrane for evaporating seawater into freshwater exclusively using solar energy, with high efficiency and large scalability. Polyimide films can be fully converted to graphene membranes using one-step laser scribing, without involving chemicals or generating wastes. These green desalination graphene membranes evaporate water at rates up to 1.37 $kg \cdot m^{-2} \cdot h^{-1}$ under one sun illumination, and possesses even higher purity than domestic water. These graphene membranes can float firmly at the air-water interface

with self-righting ability, such that the process is feasible for practical water desalination on ocean surfaces.

Introduction

Green desalination is a critical technology for solving the global water-shortage issue. Although 71% of the area of our planet is covered with seawater, freshwater scarcity is still problematic across many geological locations.[1] Currently, reverse osmosis and multi-stage flash distillation are commercially producing freshwater in many areas, such as Saudi Arabia, Israel, California, and Hong Kong. However, these methods have high electricity consumption and generate large quantities of carbon dioxide, at huge environmental expense. Evaporation, the vital part of the hydrological cycle, transforms water from liquid to gas mainly by solar radiation, 86% of which occurs over oceans.[2] However, natural solar desalination cannot yet satisfy the growing freshwater requirements due to rapid population increases and industrial expansion.

Research on novel solar desalination methods is booming, thanks to the rapid development of chemical sciences.[3] Instead of heating up the whole body of water, recent studies have demonstrated significantly higher evaporation efficiencies via the local heating of functional materials at the air-water interface.[4] Emerging materials for achieving such highly efficienct solar steam generation include metallic nanoparticles,[5] black semiconductors,[1, 6] and carbon-based materials.[7] Metallic nanoparticles take advantage of plasmonic effects, which can greatly improve the absorption of solar energy according to their corresponding resonance spectra.[8] However, these

nanoparticles are either expensive (gold, silver) or chemically vulnerable (aluminum), limiting their large-scale implantation in the oceans. Meanwhile, black semiconducting materials, such as TiO_x, can impressively evaporate water with a solar thermal conversion efficiency as high as 50% under one sun radiation[1]. However, the cost of producing such materials is too high for mass producing such solar steam generation materials, due to the use of magnesium or other expensive agents for reducing the TiO_2 nanoparticles.

Compared to metallic nanoparticles and black semiconductors, carbon-based materials are usually cheaper and have better chemical stability.[9] Porous graphene,[10] hollow graphene,[11] graphene oxide aerogel,[12] flame-treated wood,[13] carbon black,[14] etc. had already been studied for efficient solar steam generation. These emerging research achievements provide green solutions for seawater desalination exclusively using solar energy. However, the actual ocean surface is wavy and windy, and these lightweight carbon materials can be blown away or crumbled, hindering the durability of the seawater desalination process. In addition, these methods can hardly be scaled up for mass production in practical use, while maintaining a high efficiency and low cost. Carbon materials with high solar steam generation efficiencies and stable floatability are important when applying such technique in real applications.

The interesting wetting properties of lotus leaves have inspired scientists for decades into creating artificial surfaces with extraordinary wetting properties.[15-18] Various superhydrophobic surfaces have been achieved in the Cassie's or Wenzel's state via micropatterning the hydrophobic surface.[19] Recently, Jiang and coworkers also

demonstrated the outstanding air-water interface attaching ability of Janus hydrophobic/hydrophilic films with $Cu(OH)_2$ nanostructures, mimicking the lotus leaf effects.[20] However, these materials might not possess better solar steam generation performance than carbon based materials, due to their lower optical absorption and higher thermal conductivity. [21, 22] Laser scribing, with scalable fabrication ability, has been widely used for producing graphene family materials for various applications.[23, 24] Lately, there have been emerging reports on the laser synthesizing of graphene from commercial polyimide and other polymer films.[25-31] The reported graphene surfaces showed attractive wetting properties, either superhydrophobic or superhydrophobic, depending on the laser scribing environment and post treatment.[27, 32] However, synthesized carbon materials can only be found on the upper sides of polyimide films.[25, 31] The residual underlying impermeable polyimide hinders their applications for solar steam generation, not to mention possessing Janus wetting properties on the opposite surfaces. Herein, for the first time, we report a one-step laser treatment on commercial polyimide films for the mass production of carbon-based Janus superhydrophobic/superhydrophilic porous membranes, achieving excellent solar steam generation efficiency under one sun radiation. The synthesized membranes were characterized with strong solar absorption, low thermal conductivity and open porosity for capillarity, which synergistically contributes to the high performance in solar powered evaporation. In addition, the opposite sides of the synthesized membrane were superhydrophobic and superhydrophilic, realizing efficient water pumping and self-righting capabilities. Indoor and outdoor solar driven desalination experiments proved

that freshwater with a higher purity than domestic water could be generated from pristine seawater.

Experimental Section

Polyimide films (Kapton) of 25, 50, 100, 200 μm thickness from Shenzhen Ze Sheng electronic company and 50 μm thickness from Dupont were used directly after purchase. The Dupont films can be ordered worldwide, demonstrating the wide accessibility of this method, and were chosen for the following materials characterization. A DMG Lasertec 40 with 1064 nm at the CW mode was used for the laser treatment.[23] The output laser energy was measured to be 3 W with a writing speed of 400 mm/s. A Tescan MAIA3 Field Emission Scanning Electron Microscope (FESEM) with Energy Dispersive X-ray (EDX) spectroscopy was used for the morphology and elementary analysis. X-ray Photoemission Spectrometry (XPS) with a SKL-12 spectrometer and an Mg Ka X-ray source was used for the chemical information characterization. The Raman spectra was characterized with a LabRAM HR 800 Raman Spectrometer using a 488 nm laser source. The optical spectra were measured using a Perkin Elmer Lambda 650 UV-Vis spectrophotometer at 1 nm per second. The thermal conductivity was measured using an Anter Flashline 2000 Thermal Conductivity Analyzer. A Newport 91160 solar simulator (Air Mass 1.5 sunlight) was used for the evaporation test with the intensity calibrated to 1,000 W/m^2. The static contact angle was measured using a Sindatek 100SB optical contact angle meter using the sessile drop method. The electrical resistance was measured using an ISO-Tech IDM 503 multimeter. The seawater was collected at Ma Wan Island of Hong Kong.

Results and Discussion

A schematic diagram of the laser synthesis process of the graphene porous membranes is shown in **Figure 1**a. Due to the flexible nature of the commercial polyimide film, it can be directly wrapped into the roll-to-roll production process. After the 1064 nm laser scribing, the yellow polyimide turns to a black graphene film, as shown in Figure 1a. This roll-to-roll compatible process can be easily scaled up for mass production, and a typical human height length sample is shown in Figure 1b.

The selection of a 1064 nm laser for carbonizing the polyimide to graphene membranes is critical. The optical propagation of laser within the polyimide films plays a decisive role in regulating the chemical composition of the synthesized products. The actual laser intensity after entering the polyimide is given by the equation of

$$I = I_0 e^{-\frac{\alpha}{z}} \qquad \text{Equation 1}$$

where z is the penetration depth into the polyimide film, I_0 is the original intensity of laser, α is the optical absorption coefficient, which is strongly dependent on the wavelength of the laser. For a laser with wavelength at 405 nm or 10600 nm, this coefficient is relatively high. The laser energy is mostly absorbed at the top layer (facing laser directly), with almost no energy reaching the bottom part. The resulting polyimide after being treated with this laser system only has carbonized materials at the topmost layers, leaving the bottom-most part as pristine polyimide as shown in the optical image (Figure S1) and the cross-section image taken with an electrical microscope. (Figure S2 and S3). Meanwhile, the absorption coefficient α is relatively low for a laser

wavelength of 1064 nm. So sufficient energy can reach the bottom-most parts of the polyimide, and carbonize them to graphene (Figure S4 and S5). However, since the polyimide is not completely transparent for 1064 nm laser, the resulting attenuation of the light intensity can induce measurable differences in both the chemical composition and microstructure. Since polyimide contains oxygen atoms, unlike graphene, the atomic ratio of oxygen can be used for identifying the degree of polyimide carbonization. From the bottom to top side of the polyimide after 1064 nm laser treatment, the atomic ratio of oxygen increased from 1.08% to 2.95% (Figure S6 to S8), indicating less polyimide was carbonized at the bottom compared to the top layers, as illustrated in Figure 1c.

These differences of chemical compositions also result in an interesting wetting distinction. The static contact angle of the water on the top layer was almost 0^{o} as shown in Figure 1d, identified to be superhydrophilic; in contrast, the contact angle of the bottom layer is over 150^{o}, classified as superhydrophobic.[33] Further, the dynamic water interaction with sample surfaces was also studied. The superhydrophilic layer (top layer) showed instant absorbing phenomena, without water repulsion as in Figure 1e; whereas, the superhydrophobic layer (bottom layer) is repulsive to the water flow, as in Figure 1g. This Janus superwetting property equips these membranes with ultra-stable floating ability.[34] The self-righting properties of the Janus porous membranes were tested with a sample floating on water in a transparent bottle, as shown in Figure 1f-i. The sample-containing bottle was shaken, rotated, and even turned over to simulate the waves on the actual ocean surface. As expected, the flexible Janus porous membrane showed

strong anti-capsizing and surface water-proofing capability, due to the superhydrophilic bottom and superhydrophobic top surface.[20, 35] Even when the sample was immersed in the water, the superhydrophobic top layer can help float the membranes from the underneath water surfaces (Figure 4h, i). Thus, the Janus wetting properties on the opposite sides of the membranes, mimicking the lotus leaf, can provide stable floating ability at the air-water interface.

The chemical and structural properties of the synthesized graphene films were also experimentally characterized. The microstructures of the films were studied with plan-view scanning electrical microscope as shown in Figure 2. The superhydrophilic sides show obvious laser scribing patterns, with periodical porous microstructures, as shown in Figure 2a. With a close-up observation, the sizes of the pores within the graphene films were at the nanoscale, as presented in Figure 2b. The superhydrophobic sides display different morphologies, compared to the superhydrophilic sides, as shown in Figure 2c. Laser scribing patterns were not observed; instead, larger blocks of non-fully carbonized polyimide with pores were exhibited. With a zoom-in observation, the layered polyimide structures were also preserved, surrounded by the partially carbonized porous graphene flakes, as shown in Figure 2d. The different chemical compositions were also verified by XPS and Ramen spectral characterization (Figure 3). Significant less oxygen and nitrogen intensities were identified, as in Figure 3a. After being normalized with the same intensity of the C 1s peak (Figure 3b), the superhydrophilic side of the polyimide after 1064 nm laser treatment shows significantly lower intensity of the O 1s peak than the superhydrophobic side (Figure

3c). So, due to the attenuation of the polyimide according to Equation 1, less polyimide is carbonized at the superhydrophobic sides of the films, compared to the superhydrophilic sides. In addition, the difference in the superwetting states also results from the different defects ratios of the two sides. Evaluated from the molecular vibration modes, the superhydrophilic sides of the polyimide after 1064 nm laser treatment show stronger defects peaks than the superhydrophobic sides from the Raman characterization (Figure 3d). Therefore, the chemical compositions and the microstructures collectively determine the superwetting status of the graphene films.

The solar steam generating performance of the graphene membranes was studied under an indoor solar simulator with intensity calibrated at 1 $kW \cdot m^{-2}$. The highlighted graphene film floated on the water surface within a beaker, as shown in Figure 4a. The whole film area was illuminated by the solar simulator, and the overall weight of the beaker including the water and sample were measured. The weight losses against time are plotted in Figure 4b for pure water, and the graphene membranes synthesized from polyimide films with different thicknesses. The weight-loss curves for the 50 μm thick polyimide showed the highest rate at 1.37 $kg \cdot m^{-2} \cdot h^{-1}$, which is three times faster than for pure water as the control sample. And its solar steam generation efficiency is calculated. The energy conversion efficiency of solar steam generation is given as $\eta = m \cdot h_{lv}/P$, where m denotes the mass loss of water (bright field deducing dark field measured at 0.06 $kg \cdot m^{-2} \cdot h^{-1}$), h_{lv} is the liquid-to-vapor phase change enthalpy (including the sensible heat and the latent enthalpy), and P is the solar power density.[36] The evaporation rate of the Janus membranes with 50 μm thick polyimide at a power

density of 1 $kW \cdot m^{-2}$ corresponds to a solar evaporation efficiency of ~90%, which is one of the best results achieved under one sun illumination.[12, 37-39] Such high efficiency is due to the porous structures for efficient water pumping, and also the high optical absorption (Figure S9). With wavelengths ranging from 250 nm to 900 nm, the optical absorption rate was over 99.9%. Although monolayer graphene (~0.335 nm thick) possesses high optical transmission,[40] our hundreds of thousands times thicker (~90 μm thick) and randomly structured graphene membranes definitely provide a higher solar-to-thermal conversion efficiency. In addition, the porous structures contribute a low thermal conductivity (measured to be 0.045 $W \cdot m^{-1} \cdot K^{-1}$) as well as efficient water pumping channels. Locally heating the black steam generator can maximize the evaporation rates of the water (Figure S10). Thicker films have relatively high thermal insulation, yet lack sufficient microcapillary; thinner films have sufficient capillary for pumping water, however, the thermal insulating properties are compromised. As a result, the solar induced localized heating on the top of the Janus membranes with optimized thickness of 50 μm polyimide leads to the highest evaporation rate. When considering the scalability of the generators, our system also possesses the highest compatibility for direct roll-to-roll mass production, as illustrated in Figure 4c.[12, 41, 42] Such high evaporation efficiency is useful for practical applications of water vapor generation under sun illumination.

The desalination process of real seawater was also performed. For the indoor test, a smaller beaker containing the seawater and the floating graphene films (highlighted with red dash lines) for evaporation was placed on a petridish, and a larger beaker for

condensation was placed outsides with the opening facing down, as shown in Figure 5a. After being illuminated by the solar simulator for 4 hours, obvious water droplets were observed at the inner sides of the beaker and on the petridish. For outdoor testing, similar device setups were assembled, with larger beakers holding the sample, and a larger transparent glassware and a plastic basin for collecting the purified water, as shown in Figure 5c. After 4 hours, large amounts of water droplets were observed on the inner side of the collecting glassware, as shown in Figure 5d. To simply verify the purity of the purified water sourcing from the seawater, its electrical resistance was measured compared to domestic water and pristine seawater. The pristine sea water (Figure 5e), domestic water (Figure 5f), and the purified water (Figure 5g) show resistances of 2.12 MΩ, 15.5 MΩ and 21.9 MΩ, respectively. It indicates that the purified water indeed contains less electrolytes than sea water and even domestic water, showing successful desalination of seawater into freshwater.

With the continuous worldwide increase in population, the water shortage challenge will become more severe. Seawater from the ocean is an almost unlimited resource for us to use, however, the existing desalination technologies generate freshwater at high environmental and economic costs. At the same time, solar energy is unlimited and green. Making good use of solar energy for seawater desalination can sustainably provide water resources at low environmental cost.

Our work demonstrates the capability of solar energy driven desalination of seawater with roll-to-roll produced graphene membranes. The desalinated water shows even higher purity compared to drinkable domestic water. The fabricated graphene

membranes demonstrate 90% efficiency for converting solar energy and evaporate water at rate of 1.37 $kg \cdot m^{-2} \cdot h^{-1}$ under one sun illumination. The Janus superwetting membranes also attach to the air-water surface for stability when floating on the actual ocean surface. These mass production compatible graphene membranes can be easily fabricated for desalination on actual oceans.

Although some groups have reported evaporation efficiencies over 90% with several-suns illumination, the cost for such systems, including optical concentration and sun-position tracking devices, will rise significantly with large scale implantation.[43] Even though they can be used for portable devices, their freshwater generation outputs are still low compared to handy reverse osmosis (RO) devices (already commercially available on life-saving boats and hiking equipments), which can provide freshwater with a manual pumping at rate of 1 kg per minute. So, solar steam generation can only be competitive in the RO process with large scale installations, consuming solar energy rather than electricity. Since the laser writing speed can be further increased with better machines, we believe that this fabrication process can be easily scaled up for roll-to-roll mass production of such membranes. In addition, the fabricated Janus porous membranes are highly flexible and foldable. They can be rolled into small packages together with the water collection films (such as PP and PET) for areas with limited fresh water supply, and in disaster areas such as Caribbean where recently struck by Hurricane Irma and Hurricane Maria, producing freshwater from brackish water or seawater.[44] Furthermore, a recent study showed that this type of carbon generated from laser writing on polyimide possessed outstanding anti-biofouling properties, which

would lead to a long-life for such membranes operating on actual seas.[45]

Our method also shows significant advances in green chemistry than reported techniques for synthesizing solar steam generators, as compared in Table S1. The current methods usually involve hazard materials and side products during the synthesis processes. Organic solvents were usually used during the synthesis processes, and metals were frequently used as either raw materials or dealloying, which would generate considerable amounts of wastes. Acid and alkaline were also usually involved during the synthesized or post treatment processes. Solid and liquid form wastes were usually generated, decreasing the ratio of final production from the raw materials. Meanwhile, our direct polyimide to graphene synthesis is much greener, without involving any hazard materials or generating additional waste. The polyimide films can also be synthesized using green one-pot approach.[46] Although mushroom[41] and carbonized wood[38] based solar steam generators can also be considered as green methods, their scalabilities and mass production capabilities are lower than our roll-to-roll methods. Given the above aspects, our one-step method is a significant greener chemistry approach with larger scalability.

Conclusions

The Janus superhydrophobic/superhydrophilic porous membranes with self-righting, flexible and high-scalable features can be fabricated with one-step laser writing. Since the raw materials and the manufacturing facilities are both commercially available, laser direct writing in the polyimide process can be straightforwardly adapted

for roll-to-roll mass production. The flexible and light-weight membranes can be folded into rolls, which are also easy to transport and deploy. The black, porous, and relatively thick natures of these membranes provide benefit in applications for solar steam generation with high efficiencies for practical use under one-sun illumination. The materials characterization results suggest that the degree of laser induced exfoliation, as well as the laser structuring, play vital roles in determining the wetting properties, which can also inspire other applications in laser-based fabrication. These high-efficiency, scalable and Janus membranes provide a workable solution for solving the worldwide freshwater shortage challenge.

Figures

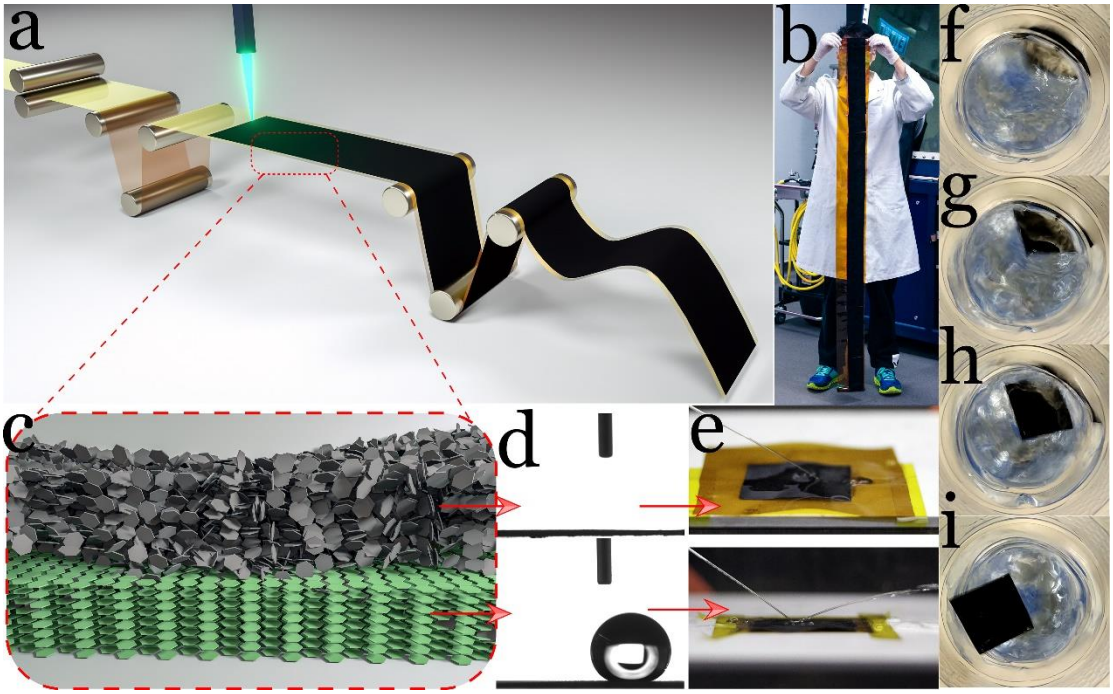

Figure 1. Synthesis and wetting properties of the laser generated graphene film. (a) Schematic illustration of the laser synthesis of Janus membrane on polyimide. (b) The optical image of the synthesized film with length at human height. (c) The schematic illustration of the Janus structured films. Static contact angle measurements of water on the top and bottom sides of the Janus membranes. (e) Dynamic water repelling image of the top and bottom sides of the Janus membranes. (f-i) The self-righting performance of Janus membranes with the superhydrophobic sides upwards, showing the sample floating out from under the water to the water surface.

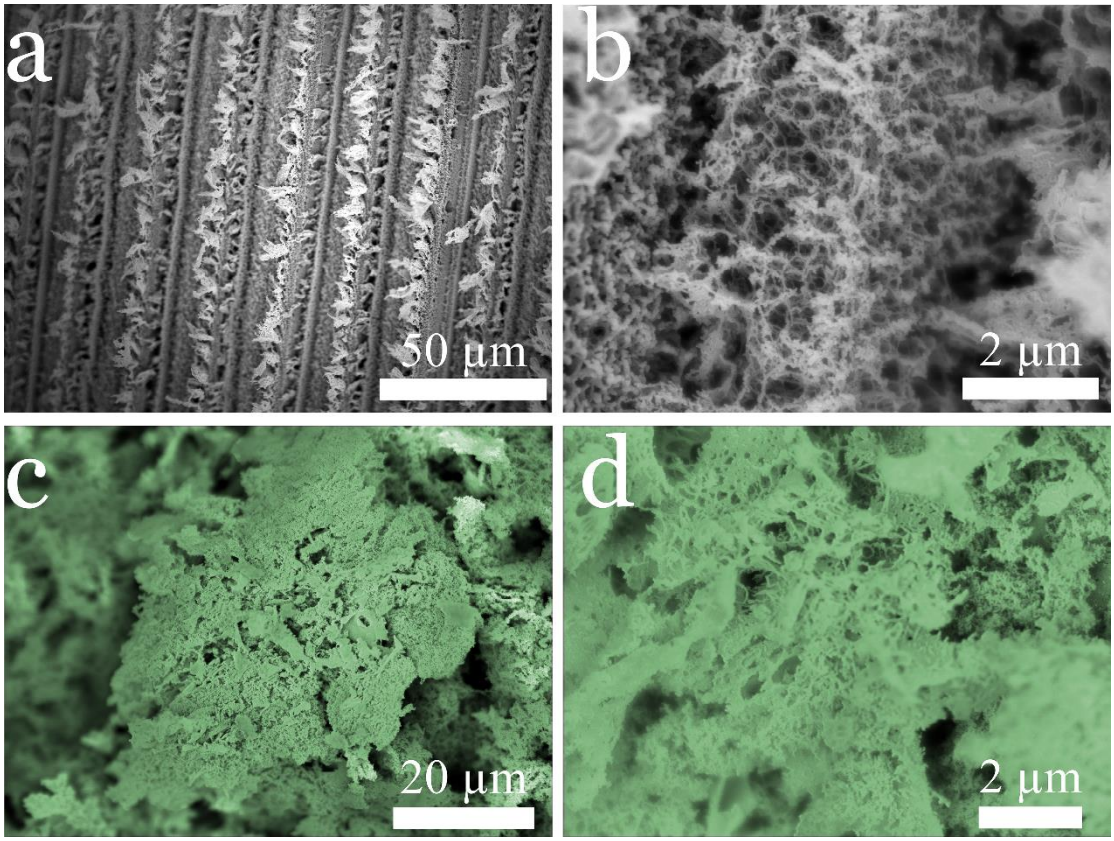

Figure 2. SEM image of the Janus membranes. Plan view SEM images of the superhydrophilic surface (a) and at higher magnification (b). Plan view SEM images of the superhydrophobic surface (c) and at higher magnification (d).

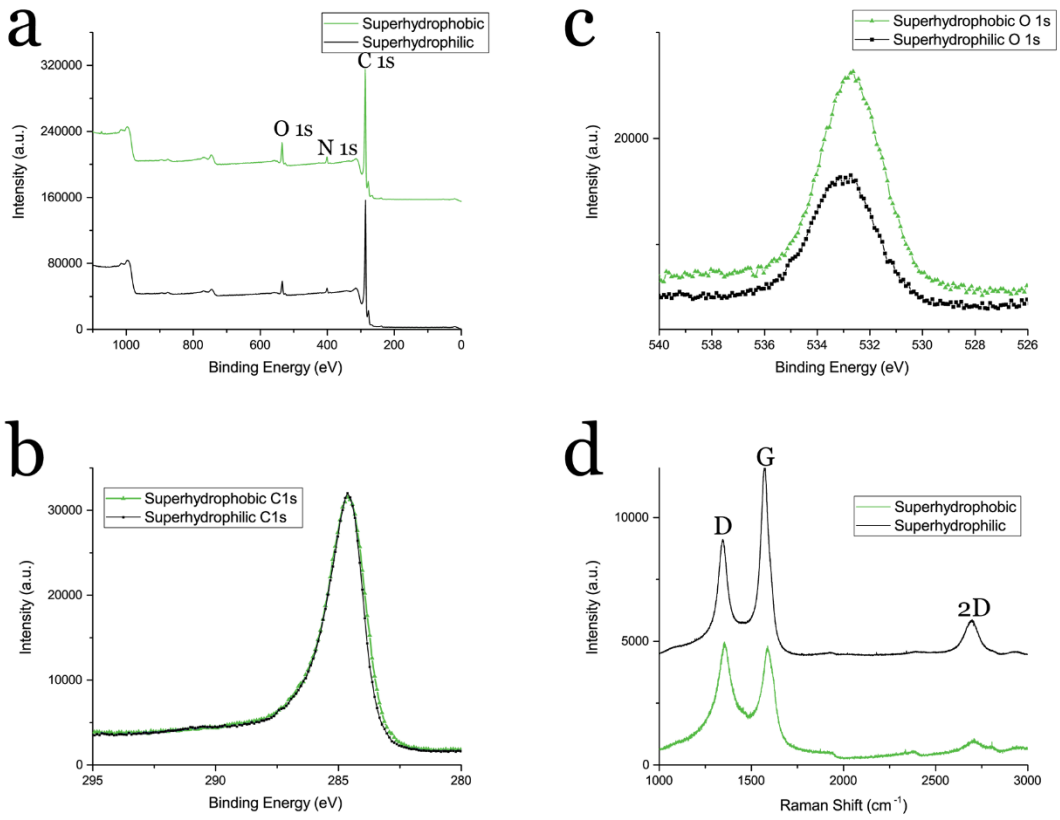

Figure 3. Spectra characterization of the Janus membrane. (a) XPS spectra of the Janus membrane with corresponding (b) C 1s and (c) O 1s peaks of the Janus membranes. (d) Raman spectra of the Janus membranes.

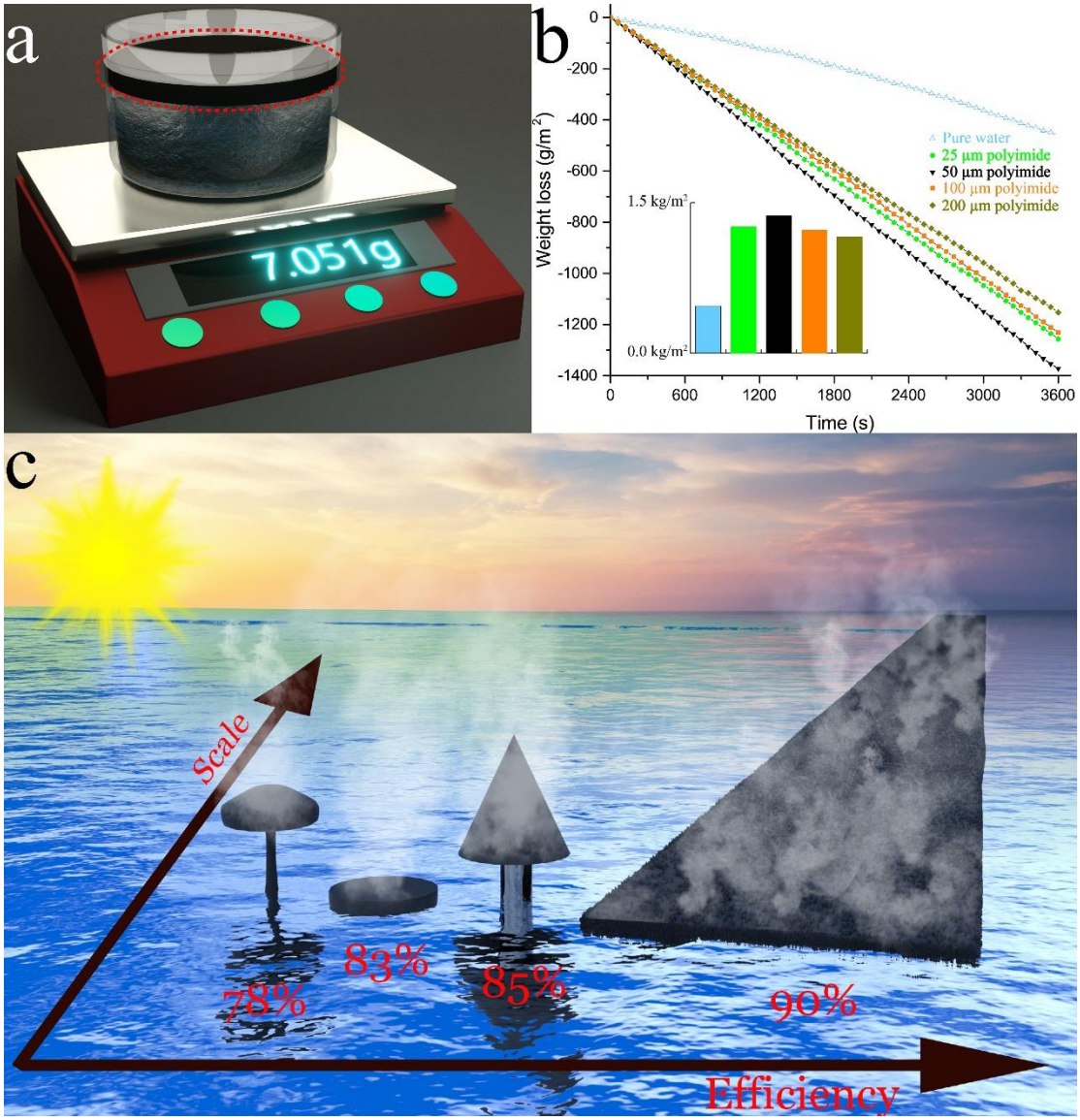

Figure 4. Steam generation performance of the Janus membranes. (a) Schematic illustration of the measurement process. (b) The evaporation mass loss of water with samples synthesized from different thicknesses of polyimide and pure water without a sample. The evaporation rates are plotted in the inset for graphene membranes synthesized from different thicknesses of polyimide. (c) Schematic diagram of the floating and self-righting Janus membranes on seawater with 90% solar evaporation efficiency under 1 sun, comparing size with other state-of-art solar steam generators: mushroom generator with 78% efficiency,[41] graphene oxide aerogel generator with 83%

efficiency,[12] and 3D artificial umbrella structured transpiration generator with 85% efficiency.[42]

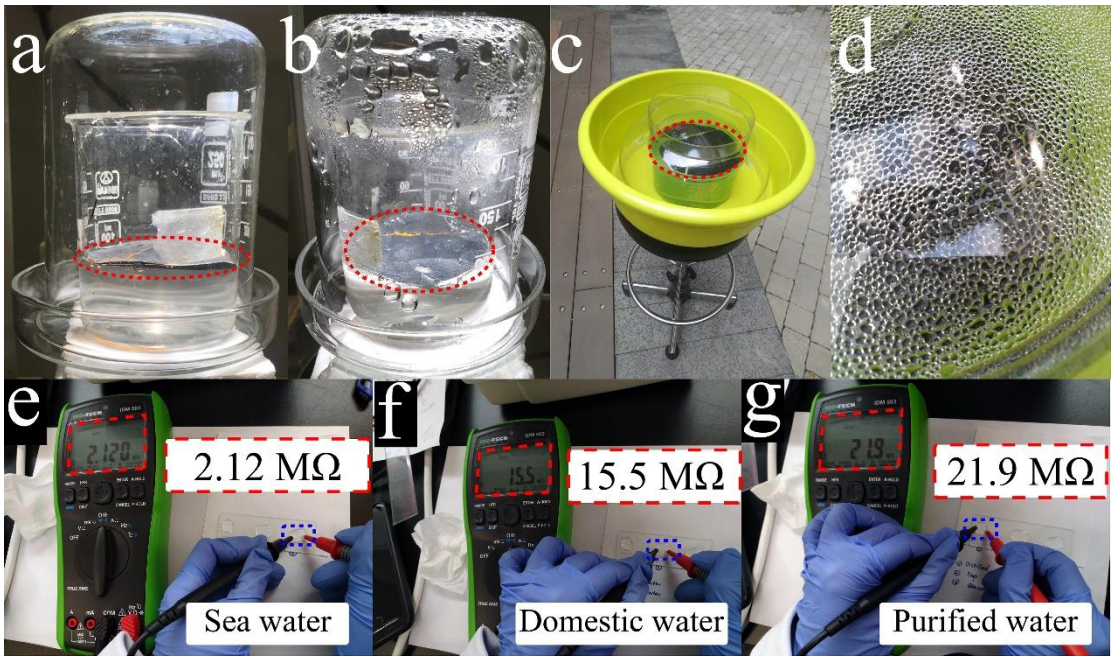

Figure 5. Seawater desalination process with the graphene membranes. Indoor seawater desalination using graphene membranes (highlighted with red dash circles) before (a) and after (b) 4 hours solar simulator. (c) Outdoor seawater desalination using graphene membranes (highlighted with red dash circles). (d) The optical image of the condensed water on the inner side of the glassware. The electrical resistance of (e) sea water, (f) domestic water, and (g) purified water, respectively.

Supporting Information

Supporting Information is available from the authors. The video abstract is available on YouTube at: https://youtu.be/ZFoypUiH0GE

Acknowledgements

The project was funded by the Postdoctoral Fellowship Scheme of the Hong Kong Polytechnic University with project number G-YW2R. Prof. Law acknowledged The Hong Kong Polytechnic University (1-ZVJ5) and the National Natural Science Foundation of China (NSFC) (61405169).

Conflict of Interest

The authors declare no conflict of interest.

Keywords: desalination, sustainable, graphene, solar energy, superhydrophobic

References

1. M. M. Ye, J. Jia, Z. J. Wu, C. X. Qian, R. Chen, P. G. O'Brien, W. Sun, Y. C. Dong and G. A. Ozin, *Adv. Energy Mater.*, 2017, **7**, 1601811.
2. H. Y. Ren, M. Tang, B. L. Guan, K. X. Wang, J. W. Yang, F. F. Wang, M. Z. Wang, J. Y. Shan, Z. L. Chen, D. Wei, H. L. Peng and Z. F. Liu, *Adv. Mater.*, 2017, **29**, 1702590.
3. G. Ni, G. Li, S. V. Boriskina, H. X. Li, W. L. Yang, T. J. Zhang and G. Chen, *Nat. Energy*, 2016, **1**, 16126.
4. C. J. Chen, Y. J. Li, J. W. Song, Z. Yang, Y. Kuang, E. Hitz, C. Jia, A. Gong, F. Jiang, J. Y. Zhu, B. Yang, J. Xie and L. B. Hu, *Adv. Mater.*, 2017, **29**, 1701756.
5. L. Zhou, Y. L. Tan, J. Y. Wang, W. C. Xu, Y. Yuan, W. S. Cai, S. N. Zhu and J. Zhu, *Nat. Photonics*, 2016, **10**, 393-399.
6. J. Wang, Y. Y. Li, L. Deng, N. N. Wei, Y. K. Weng, S. Dong, D. P. Qi, J. Qiu, X. D. Chen and T. Wu, *Adv. Mater.*, 2017, **29**, 1603730.
7. X. Q. Li, W. C. Xu, M. Y. Tang, L. Zhou, B. Zhu, S. N. Zhu and J. Zhu, *Proc. Natl. Acad. Sci. U. S. A.*, 2016, **113**, 13953-13958.
8. L. Zhou, Y. L. Tan, D. X. Ji, B. Zhu, P. Zhang, J. Xu, Q. Q. Gan, Z. F. Yu and J. Zhu, *Sci. Adv.*, 2016, **2**, e1501227.
9. P. P. Zhang, J. Li, L. X. Lv, Y. Zhao and L. T. Qu, *ACS Nano*, 2017, **11**, 5087-5093.
10. Y. Ito, Y. Tanabe, J. H. Han, T. Fujita, K. Tanigaki and M. W. Chen, *Adv. Mater.*, 2015, **27**, 4302-4307.

11. J. G. Zhou, Z. L. Sun, M. Q. Chen, J. T. Wang, W. M. Qiao, D. H. Long and L. C. Ling, *Adv. Funct. Mater.*, 2016, **26**, 5368-5375.

12. X. Z. Hu, W. C. Xu, L. Zhou, Y. L. Tan, Y. Wang, S. N. Zhu and J. Zhu, *Adv. Mater.*, 2017, **29**, 1604031.

13. K. K. Liu, Q. Jiang, S. Tadepallifit, R. Raliya, P. Biswas, R. R. Naik and S. Singamaneni, *ACS Appl. Mater. Interfaces*, 2017, **9**, 7675-7681.

14. Y. Liu, J. Chen, D. Guo, M. Cao and L. Jiang, *ACS Appl. Mater. Interfaces*, 2015, **7**, 13645-13652.

15. D. M. Zang, R. W. Zhu, W. Zhang, X. Q. Yu, L. Lin, X. L. Guo, M. J. Liu and L. Jiang, *Adv. Funct. Mater.*, 2017, **27**, 1605446.

16. L. Jiang, Y. Zhao and J. Zhai, *Angew. Chem.*, 2004, **43**, 4338-4341.

17. Y. W. Wu, T. Hang, Z. Y. Yu, L. Xu and M. Li, *Chem. Commun. (Camb.)*, 2014, **50**, 8405-8407.

18. H. L. Yang, F. X. Liang, Y. Chen, Q. Wang, X. Z. Qu and Z. Z. Yang, *NPG Asia Mater.*, 2015, **7**, e176.

19. A. Lafuma and D. Quere, *Nat. Mater.*, 2003, **2**, 457-460.

20. Y. Y. Zhao, C. M. Yu, H. Lan, M. Y. Cao and L. Jiang, *Adv. Funct. Mater.*, 2017, **27**, 1701466.

21. W. K. C. Yung, B. Sun, J. Huang, Y. Jin, Z. Meng, H. S. Choy, Z. Cai, G. Li, C. L. Ho, J. Yang and W. Y. Wong, *Sci. Rep.*, 2016, **6**, 31188.

22. W. K. C. Yung, B. Sun, Z. Meng, J. Huang, Y. Jin, H. S. Choy, Z. Cai, G. Li, C. L. Ho, J. Yang and W. Y. Wong, *Sci. Rep.*, 2016, **6**, 39584.

23. W. K. C. Yung, G. Li, H. M. Liem, H. S. Choy and Z. Cai, *J. Mater. Chem. C*, 2015, **3**, 11294-11299.

24. X. Dai, J. Wu, Z. C. Qian, H. Y. Wang, J. Jian, Y. J. Cao, M. H. Rummeli, Q. H. Yi, H. Y. Liu and G. F. Zou, *Sci. Adv.*, 2016, **2**, e1601574.

25. J. Lin, Z. W. Peng, Y. Y. Liu, F. Ruiz-Zepeda, R. Q. Ye, E. L. G. Samuel, M. J. Yacaman, B. I. Yakobson and J. M. Tour, *Nat. Commun.*, 2014, **5**, 5714.

26. L. Q. Tao, H. Tian, Y. Liu, Z. Y. Ju, Y. Pang, Y. Q. Chen, D. Y. Wang, X. G. Tian, J. C. Yan, N. Q. Deng, Y. Yang and T. L. Ren, *Nat. Commun.*, 2017, **8**, 14579.

27. A. Lamberti, F. Clerici, M. Fontana and L. Scaltrito, *Adv. Energy Mater.*, 2016, **6**, 1600050.

28. L. Li, J. B. Zhang, Z. W. Peng, Y. L. Li, C. T. Gao, Y. S. Ji, R. Q. Ye, N. D. Kim, Q. F. Zhong, Y. Yang, H. L. Fei, G. D. Ruan and J. M. Tour, *Adv. Mater.*, 2016, **28**, 838-845.

29. Z. W. Peng, R. Q. Ye, J. A. Mann, D. Zakhidov, Y. L. Li, P. R. Smalley, J. Lin and J. M. Tour, *ACS Nano*, 2015, **9**, 5868-5875.

30. A. Lamberti, M. Serrapede, G. Ferraro, M. Fontana, F. Perrucci, S. Bianco, A. Chiolerio and S. Bocchini, *2D Materials*, 2017, **4**, 035012.

31. J. B. In, B. Hsia, J.-H. Yoo, S. Hyun, C. Carraro, R. Maboudian and C. P. Grigoropoulos, *Carbon*, 2015, **83**, 144-151.

32. Y. L. Li, D. X. Luong, J. B. Zhang, Y. R. Tarkunde, C. Kittrell, F. Sargunaraj, Y. S. Ji, C. J. Arnusch and J. M. Tour, *Adv. Mater.*, 2017, **29**, 1700496.

33. X. L. Tian, T. Verho and R. H. A. Ras, *Science*, 2016, **352**, 142-143.

34. M. R. Song, J. Ju, S. Q. Luo, Y. C. Han, Z. C. Dong, Y. L. Wang, Z. Gu, L. J. Zhang, R. R. Hao and L. Jiang, *Sci. Adv.*, 2017, **3**, e1602188.

35. L. Li, Y. Bai, L. Li, S. Wang and T. Zhang, *Adv. Mater.*, 2017, **29**, 1702517.

36. H. Ghasemi, G. Ni, A. M. Marconnet, J. Loomis, S. Yerci, N. Miljkovic and G. Chen, *Nat. Commun.*, 2014, **5**, 4449.

37. Q. S. Jiang, L. M. Tian, K. K. Liu, S. Tadepalli, R. Raliya, P. Biswas, R. R. Naik and S. Singamaneni, *Adv. Mater.*, 2016, **28**, 9400-9407.

38. M. Zhu, Y. Li, G. Chen, F. Jiang, Z. Yang, X. Luo, Y. Wang, S. D. Lacey, J. Dai, C. Wang, C. Jia, J. Wan, Y. Yao, A. Gong, B. Yang, Z. Yu, S. Das and L. Hu, *Adv. Mater.*, 2017, **29**, 1704107.

39. P. D. Dongare, A. Alabastri, S. Pedersen, K. R. Zodrow, N. J. Hogan, O. Neumann, J. J. Wu, T. X. Wang, A. Deshmukh, M. Elimelech, Q. L. Li, P. Nordlander and N. J. Halas, *Proc. Natl. Acad. Sci. U. S. A.*, 2017, **114**, 6936-6941.

40. K. S. Kim, Y. Zhao, H. Jang, S. Y. Lee, J. M. Kim, K. S. Kim, J. H. Ahn, P. Kim, J. Y. Choi and B. H. Hong, *Nature*, 2009, **457**, 706-710.

41. N. Xu, X. Z. Hu, W. C. Xu, X. Q. Li, L. Zhou, S. N. Zhu and J. Zhu, *Adv. Mater.*, 2017, **29**, 1606762.

42. X. Li, R. Lin, G. Ni, N. Xu, X. Hu, B. Zhu, G. Lv, J. Li, S. Zhu and J. Zhu, *National Science Review*, 2017, **5**, 70-77.

43. J. M. Gordon and H. T. Chua, *Nat. Photonics*, 2017, **11**, 70-70.

44. J. S. Ramírez Lugo and C. A. Torres-Ramos, *Science*, 2017, **358**, 151-151.

45. S. P. Singh, Y. L. Li, A. Be'er, Y. Oren, J. M. Tour and C. J. Arnusch, *ACS Appl. Mater. Interfaces*, 2017, **9**, 18238-18247.

46. L. Leimhofer, B. Baumgartner, M. Puchberger, T. Prochaska, T. Konegger and M. M. Unterlass, *Journal of Materials Chemistry A*, 2017, **5**, 16326-16335.